

BlackBox: Generalizable Reconstruction of Extremal Values from Incomplete Spatio-Temporal Data

Tomislav Ivek · Domagoj Vlah

Received: 30 April 2020 / Accepted: date

Abstract We describe our submission to the Extreme Value Analysis 2019 Data Challenge in which teams were asked to predict extremes of sea surface temperature anomaly within spatio-temporal regions of missing data. We present a computational framework which reconstructs missing data using convolutional deep neural networks. Conditioned on incomplete data, we employ autoencoder-like models as multivariate conditional distributions from which possible reconstructions of the complete dataset are sampled using imputed noise. In order to mitigate bias introduced by any one particular model, a prediction ensemble is constructed to create the final distribution of extremal values. Our method does not rely on expert knowledge in order to accurately reproduce dynamic features of a complex oceanographic system with minimal assumptions. The obtained results promise reusability and generalization to other domains.

Keywords Convolutional neural network · Data reconstruction · Deep learning · Extreme Value Analysis Conference challenge · Ensemble · Spatio-temporal extremes

1 Introduction

The EVA 2019 Data Challenge posited a problem to predict extremes of the Red Sea surface temperature anomaly within spatio-temporal regions of missing data Huser (2020). Daily temperature anomaly values were provided for

Tomislav Ivek
Institut za fiziku, Bijenička 46, HR-10000 Zagreb, Croatia
E-mail: tivek@ifs.hr

Domagoj Vlah
University of Zagreb, Faculty of Electrical Engineering and Computing, Department of Applied Mathematics, Unska 3, HR-10000 Zagreb, Croatia
E-mail: domagoj.vlah@fer.hr

contestants spanning over 31 years and covering the geographical area of the Red Sea. For each day, temperature anomaly values were given at fixed spatial points on a regular geographical grid. About 31.6% of data was deliberately removed from the dataset. Regions of the missing data were approximately contiguous with irregular boundaries, relatively large, at least one calendar month in duration, and present for every calendar day in the provided dataset. The exact process of data removal was not disclosed to contestants. The goal was to predict the distribution of extremes of temperature anomaly on a number of specified space-time cylindrical regions (50km in radius and 7 days in length), chosen in the most difficult part of the dataset which had 60% percent of data missing for any day. The quality of predicted extremes was evaluated using threshold-weighted continuous ranked probability score twCRPS averaged over all prediction regions.

In the absence of expert domain knowledge, to predict the distribution of extremes of Red Sea surface temperature anomaly within regions of withheld data we attempt to reconstruct the missing information. We introduce additional damage in order to teach autoencoder-like models based on convolutional deep neural networks how to repair the missing data. Then, we apply trained models on originally provided data in order to create stochastic plausible reconstructions of temperature anomaly within regions of missing data. The extremal values within regions of interest are then trivially calculated for each stochastically sampled reconstruction which finally allows us to create their distribution. We discuss details of our implementation, possible extensions to the technique and its generalizability to different problem domains.

2 Overview of related work

We first review some of the recently published techniques based on neural networks relevant to missing data reconstruction. Neural networks are parameterizable approximators based on multiple compositions of affine and nonlinear functions which are fitted to, or trained on, some desired dataset. They have long been used to recover data gaps in time series, including geophysical datasets (Rossiev et al. 2002; Lee and Park 2015). Conventionally, raw data is first reduced and mapped onto a small-dimension manifold, also called latent or hidden space, which aims to capture salient features underlying the modeled phenomena. In case of time series, latent vectors are then reconstructed at missing time stamps by a neural network predicting the next step based on history. Finally, the predicted reconstruction is projected back to original data space. Various model architectures are researched here and used in production, most common being simple fully connected networks (Rossiev et al. 2002), recurrent neural networks (Che et al. 2018), which are either fully-connected for tabular data or combined with convolutional neural networks where spatial or temporal proximity is important (Asadi and Regan 2019). Particularly interesting is the recently introduced BRITS architecture (Cao et al. 2018), which uses a novel bidirectional recurrent component based on learned feature

correlation and temporal decay in order to impute data. While this technique seems most promising for tabular data with measured or engineered features of interest, it needs to be adapted in order to handle image-like data on a large spatial grid.

Since the number of parameters of neural layers grows proportionally to dimensionality of their input, fully connected neural networks where each element of input influences the whole of output are often deemed intractable for large image-like inputs. Moreover, in computer vision and image processing it is commonly desirable that algorithms operate independently of feature position, eg., a face detection network should correctly identify human faces regardless of their position in a photograph. With this in mind, convolutional neural networks (Zhang 1988) have become the prevalent choice for modeling ordered data on space-like grids. Such an architecture again comprises layers, each with a small common neural network, or “kernel”, which slides over the whole input. Output of a convolutional layer can be regarded as a spatial map of detected learnable features which grows semantically richer with every consecutive layer. Thanks to their shared-weight architecture and local connectivity (Behnke 2003), convolutional neural networks train well on smaller datasets, generalize to unseen data examples, and are used with great success in various classification and prediction tasks (Krizhevsky et al. 2012; Schlemper et al. 2017).

Recently an innovative convolutional framework was proposed for missing data reconstruction called MisGAN (Li et al. 2019). It is particularly suited for high-dimensional data with underlying spatial correlations. MisGAN uses multiple generative adversarial networks (Goodfellow et al. 2014) where the so-called generators create increasingly more convincing fake samples as well as their missing data masks, while the discriminators attempt to discern them from real samples. This complex scheme simultaneously learns the distribution of missing data, or “masks”, as well as the conditional distribution of data predicated on masks. It finally constructs a probabilistic imputer model which repairs the data by sampling from the learned distribution given some known data and its mask.

MisGAN provides state-of-the-art reconstruction results on several standard datasets and appears to be particularly suited to the task at hand. However, in our preliminary experiments to apply MisGAN on Red Sea temperature anomalies it was difficult to achieve suitable convergence. Generative adversarial networks are notoriously difficult to train as they are a minmax problem where the optimal state is a saddle point with a local minimum in generator network cost and local maximum of the discriminator network cost (Wei et al. 2018; Le et al. 2017). In our admittedly limited tests, MisGAN tended to diverge and create patterned artifacts. Furthermore, the training itself took prohibitive amounts of time while it also appeared the provided amount of data was not sufficient.

Due to these issues, for the particular problem of Red Sea temperature anomalies we opt to step back from generative adversarial networks and construct a simpler framework based on autoencoder networks (Kramer 1991;

Goodfellow et al. 2016). Still, MisGAN provides us with certain valuable tools and avenues to explore. We adopt its use of noise-imputed samples in order to treat trained models as conditional distributions. Also, we use a simpler version of convolutional networks to exploit spatial coherence and short-range temporal correlations. We forego long-term dependencies and leave them for future consideration.

3 Model and methodology

We aim to construct one or more models which would take as input incomplete, damaged temperature anomaly data and attempt its best guess to reconstruct or predict the original complete data. In the following section we introduce separate “ingredients” which come together to form a powerful framework for probabilistic data repair.

3.1 Trivial case: target data is complete and available for model training

Starting with the most simple case, let us for now disregard time dependence of temperature anomaly data and consider each day as a separate multi-dimensional point. Suppose we have the desired input-output relations $\{(x_{\text{orig}}^{(n)}, y_{\text{complete}}^{(n)}); n \in [1, \dots, N]\}$, where $x_{\text{orig}}^{(n)}$ is a vector representing originally incomplete or damaged data provided in the problem statement and $y_{\text{complete}}^{(n)}$ the ideal, undamaged data for each day n . If θ designates all the parameters of some model attempting to summarize these relations, their optimal value to reconstruct the missing data based on $x_{\text{orig}}^{(n)}$ as input can be obtained by minimizing the loss function

$$\mathcal{L} = \frac{1}{N} \sum_{n=1}^N \ell(y_{\text{complete}}^{(n)}; o^{(n)}(\theta)) \quad (1)$$

where $o^{(n)}(\theta)$ is the model output predicated on parameters θ for model input $x_{\text{orig}}^{(n)}$ and ℓ is a suitable distance function between targets and corresponding model outputs.

Inconveniently, the complete data $y_{\text{complete}}^{(n)}$ is unavailable to us by the very nature of the problem we wish to solve. Moreover, the posited Data Challenge could in principle be solved by optimizing the twCRPS score but the scoring function is specifically not available to contestants. Therefore, a working solution will necessarily grow more complex as we need to find an adequate proxy cost function to minimize.

3.2 Extracting salient information by introducing additional damage

The provided daily temperature anomaly data on a geographical grid can be regarded as a time series of raster images represented by real matrices

with W columns in width and H rows in height where each matrix element corresponds to the value of temperature anomaly at a certain geolocation for day n . We introduce its masking matrix $m_{\text{orig}}^{(n)}$ of the same shape which describes the extent of damage present in $x_{\text{orig}}^{(n)}$. It carries binary information for each spatial location: 1 encodes that a value is observed and available and 0 designates unobserved values eg. due to damage or the location itself not being present in the dataset (Cao et al. 2018; Li et al. 2019).

Let us now introduce additional data loss to the already damaged original data. We describe the total damage, ie. newly introduced damage together with the originally missing data, in the form of a new binary masking matrix $m'^{(n)}$. The additionally damaged data matrix then becomes

$$x'^{(n)} = x^{(n)} \odot m'^{(n)}, \quad (2)$$

where \odot denotes element-wise multiplication of two matrices.

This setup in principle allows us to train a model which maps data with additional damage $x'^{(n)}$ onto the data with original amount of damage as the target, $y'^{(n)} = x_{\text{orig}}^{(n)}$. Our main idea is that by training to repair the additional damage, a sufficiently powerful convolutional model could learn to extract features underpinning the data manifold which are robust to damage. Then, when such a trained model is applied to the original data, we hypothesize it will be able to reconstruct missing data in an adequate manner.

3.3 Weighted distance function

The training goal also needs to codify that the relevant cost is evaluated only where data is provided by the inherently damaged training target. For the distance function ℓ in (1) we substitute weighted L^1 or L^2 distances evaluated exclusively on the original masks $m_{\text{orig}}^{(n)}$ so that missing or unobserved data is ignored:

$$\ell\left(y^{(n)}, m_{\text{orig}}^{(n)}; o^{(n)}\right) = \frac{\left\| \left(y^{(n)} - o^{(n)}\right) \odot m_{\text{orig}}^{(n)} \right\|_{1,2}}{\sum m_{\text{orig}}^{(n)}}. \quad (3)$$

Here $\|\cdot\|_{1,2}$ denotes L^1 or L^2 norm and the sum in the denominator is performed over all mask elements, effectively counting the number of observed temperature anomaly values in a particular day. Note that the computation of $o^{(n)}$ requires additionally damaged data $x'^{(n)} = x^{(n)} \odot m'^{(n)}$, but the distance ℓ being minimized in (3) utilizes the original mask $m_{\text{orig}}^{(n)}$.

With such modifications in place, the training procedure will create models that reproduce known data but are not punished when “speculating” on regions of missing data.

3.4 Sampling from trained models as multivariate probability distributions

We found it most fruitful to introduce both a level of stochasticity to model training input, as well as to the evaluation input fed into trained models. Specifically, we impute noise wherever masks indicate missing data:

$$x_{\text{noise}}^{(n)} = \left[x^{(n)} \odot m'^{(n)} + \mathcal{N} \odot (1 - m'^{(n)}) \right] \odot m_{\text{master}}, \quad (4)$$

$$x_{\text{orig,noise}}^{(n)} = \left[x^{(n)} \odot m_{\text{orig}}^{(n)} + \mathcal{N} \odot (1 - m_{\text{orig}}^{(n)}) \right] \odot m_{\text{master}}, \quad (5)$$

where \mathcal{N} is noise sampled separately for each spatio-temporal location and m_{master} is the master mask with 1 at every valid spatial location and 0 otherwise which effectively removes any noise spilling outside of the valid geographical Red Sea region.

Setting the distribution of imputed noise \mathcal{N} equal to the expected distribution of missing data allows the model to learn expected ranges of valid data within the damaged regions. Moreover, imputed noise in evaluation input allows us to stochastically sample from the trained model, effectively using it as a multivariate conditional probability distribution. Such a sampling procedure has the most desirable property that the dimensionality of noise is proportional to the amount of data loss: the more information the model receives as input, the less variation it creates at its output (Li et al. 2019).

3.5 Convolutional autoencoder architecture

Finally, we describe a flexible family of parameterizable functions with sufficient capacity to learn patterns inherent to the provided incomplete matrix data and provide reasonable reconstructions of the complete pristine data. The models we employ are simple, sequential convolutional neural networks and almost symmetric encoder and decoder parts. Extensive use of the convolution operation allows models to detect and utilize any inherent spatial correlations. Each encoder layer consists of a linear convolution operation and a nonlinear function.

Figure 1 shows the architecture of the convolutional model. The first layer of the network takes as input tensors of general shape $d_{\text{in}} \times W \times H$, that is $W \times H$ matrix data with d_{in} dimensionality or “channels”. This very first layer increases the number of channels at its output to d_{ch} which is preserved by subsequent layers. The following N_{outer} encoder layers do not change the spatial size of the tensor, however the next N_{reduce} layers each reduce the spatial extents of data by a factor of 2 using convolutions of stride 2. Finally, the last set of N_{inner} encoder layers again preserve tensor shape and generate the latent space result. The decoder closely follows this architecture in reverse using transposed convolutions instead of convolutions and ends with an additional single transposed convolution which outputs an one-channel tensor that is a matrix corresponding to reconstructed temperature anomaly.

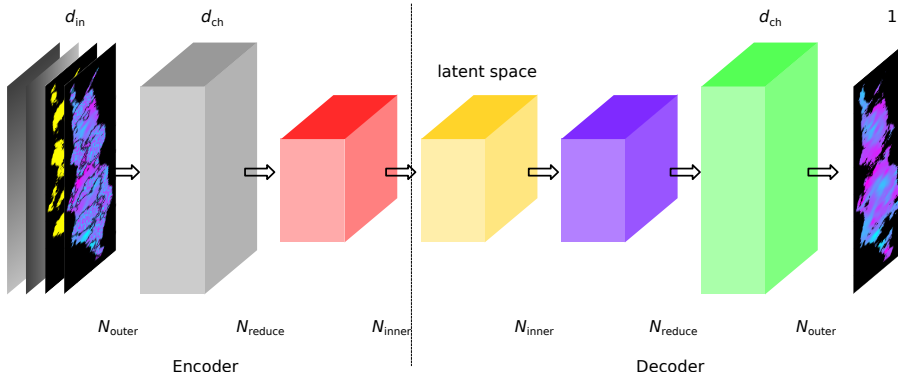


Fig. 1 Architecture of the convolutional autoencoder model. At encoder input a tensor with d_{in} channels is given containing several days worth of data (training data depicted, see text). The first block of N_{outer} convolutional layers increase the number of channels to d_{ch} . Then, N_{reduce} layers reduce the spatial extents of the tensor. Following those, N_{inner} convolutional layers map the tensor into latent space. The decoder structure is approximately symmetric to the encoder. The model outputs a single-channel tensor as prediction.

We allow this architecture to use a block consecutive days as input by setting $d_{in} > 1$. Inspecting several days of data to reconstruct a single day’s temperature anomaly exploits short-term temporal correlations inherent to oceanographic data and teaches the model to also use rates of change instead of separate “snapshots” at a single point in time.

One typical advantage of convolutional neural networks, translational invariance, can become a hindrance when data might depend on absolute position in space. In our case, it may very well be that Red Sea temperature anomalies consistently differ depending on geographical location. Inspired by recent developments in natural language processing (Vaswani et al. 2017), we add two more channels to the input which encode absolute geographical longitude and latitude of each point. In this way a model might find it advantageous to use positional information for greater selectivity and more precise predictions.

3.6 Training protocol and implementation

Our model, training and evaluation code is available online at <https://github.com/BlackBox-EVA2019/BlackBox>.

Training dataset and validation dataset. In order to train our models we separate the provided data $(x_{orig}^{(n)}, m_{orig}^{(n)})$, per day basis, into two datasets, named (as customary in machine learning model) the training and the validation dataset. The training dataset is used to train models. Validation dataset is used during model development to measure the generalization capability of

models on unseen data. Finally, the test set, data withheld from contest participants, is not available to us and was not used for model training purposes or optimization of model architecture.

Only after the models are trained and evaluated, we calculate the $\overline{\text{twCRPS}}$ score of our final predictions using the observed distribution of extremal values which was provided by the contest organizers after the final ranking was determined.

Notice here the important difference between our naming scheme and the one in the Data Challenge problem statement Huser (2020). In the problem statement, the whole available data $x_{\text{orig}}^{(n)}$ where $m_{\text{orig}}^{(n)} = 1$ is called the training dataset, and the subset of rest of the data hidden to contestants where $m_{\text{orig}}^{(n)} = 0$ but $m_{\text{master}}^{(n)} = 1$ is called the validation dataset.

Not all days in the Red Sea dataset have the same amount of non-missing data. The available time window spans over a total of 31 years, but for the first 22 years 20% of data per day is missing, and for the last 9 years 60% of data per day is missing. Incidentally, the latter 9 years with more missing data also represents the period of accelerated climate change. The validation set has to be representative of all data, so we choose it as 5 continuous years where 22/31 parts are from the first 22 years and 9/31 parts are from the last 9 years, ie. data belonging from 6736th to 8560th day. The remaining data is used for the training set. In this way both our training and validation datasets consist of large contiguous blocks of time, have the same distribution of missing data percentage, and potentially both contain data from the period of accelerated climate change.

Generating additional masks. Regarding the model training process, as already stated in Section 3, we introduce further damage to the data for training input. A nontrivial question is how much additional data we should mask. We consider the natural choice to mask the same percentage of data for the process of training as would be masked during model inference when generating predictions of unknown test data. In the last 9 years of data, where we are tasked to generate predictions, 60% of data is masked. Therefore we need to create masks $m'^{(n)}$ such that approximately 60% percent of data is removed for each day in training and validation datasets. Notice that the total data loss by masking $m'^{(n)}$ is 68% for the first 22 years of data, and even 84% for the last 9 years!

A further issue is how to actually generate masks $m'^{(n)}$. Our limited experiments with training generative adversarial networks (Li et al. 2019) to create convincing masks did not produce desired results. Therefore it is important to devise a method to create adequate masks $m'^{(n)}$. Except noting that $m_{\text{orig}}^{(n)}$ change once only every calendar month so our generated masks need to do the same, the exact mechanism by which $m_{\text{orig}}^{(n)}$ were generated is unknown to us. We used a stochastic diffusion algorithm that generates masks similar in appearance to those provided by problem statement. Our algorithm needed

to be tweaked until generated masks looked acceptable which is certainly one obvious drawback of our method.

Noise imputation. The imputed noise is sampled from a Gaussian distribution closely mimicking the marginal distribution of all provided temperature anomaly measurements, parameterized by $\mu = -0.0365^\circ\text{C}$ and $\sigma = 0.683^\circ\text{C}$.

Reducing the data footprint. The original anomaly data is spatially large and taxes the capacity of current GPU architectures, both in sense of used memory and computation time. We used two complementary approaches to successfully reduce the GPU footprint.

Using only a small number of padding rows and columns at the edges, the original temperature anomaly data fits into a spatial matrix of $W \times H = 256 \times 384$. Notice that 256 is a power of 2 and 384 is 3 times a power of 2, which turns out to be essential for efficient computation with convolutions. However, note that the Red Sea is elongated but geographically laying in the direction NNW-SSE so in our rectangular image representation most image elements correspond to land masses which carry no relevant data.

In order to increase the density of usable data we skew every other image row together with remaining rows below it towards west, beginning from the top to the bottom of image. In this way the whole Red Sea can fit in an image $W \times H = 96 \times 384$, while still preserving spatial coherence. At this point the data size is reduced but still leaves an unacceptably large GPU footprint.

Further, notice that our skew operation results with spatial extents of 96×384 which are divisible by 3. We can conveniently down-sample the data by taking the average anomaly value over 3×3 spatial cells which brings the data size down by almost an order of magnitude, a quite substantial amount. We get the final anomaly matrix resolution of $W \times H = 32 \times 128$. Both numbers are factors of 2 which is suitable for efficient GPU computations. Our models are both trained and inferred in this lower resolution.

To generate a prediction from a model trained on such data, after inference with reduced resolution we have to first upsample and then unskew rows back to original position. Upsampling is done using bicubic interpolation. Special care is taken at the boundary of masks in order to avoid issues with fractional data availability and oscillation artifacts in the reconstruction of high resolution data near mask boundaries. The error introduced by resampling, measured by L^1 loss function (1) and (3) on the whole dataset, is 0.012, which is much smaller than the mean values of L^1 validation loss function obtained during model training, which is 0.020. This provides evidence that the error introduced by computation on downsampled data is less significant in comparison to the inherent error introduced from our models.

Convolutional autoencoder hyperparameters. The described model is implemented in Python using the PyTorch library (Paszke et al. 2019). For the encoder part we used from 2 to 11 layers, so after the first “expanding” layer

which changes the number of channels from d_{in} to d_{ch} we have 1 to 10 additional outer, reducing and inner layers. So $1 \leq N_{outer} + N_{reduce} + N_{inner} \leq 10$, where we prescribe $N_{outer} \geq 1$ and $N_{reduce} \leq 5$. The latter is because after downsampling we have $W = 32 = 2^5$, which means that we can include at most 5 layers that reduce spatial size by a factor of 2 each. As explained before, the decoder part is symmetrical having an additional one output convolution layer without nonlinear activation function. So the total number of layers in our convolutional autoencoder is between 5 and 23 layers, not counting the additional dropout layer (Nitish et al. 2014) that we add between the encoder and decoder parts. Dropout proves necessary to reduce overfitting during training. Dropout percentage is an optimizer hyperparameter that we discuss further below.

For the number of channels we take $d_{ch} = 64$ and the convolution kernel size we fix at 5×5 . In every convolutional layer except last we use the SELU activation function (Klambauer et al. 2017). The last layer is purely affine and without an activation function. Also, each convolutional layer except last uses a batch normalization layer after activation function, as it improves training convergence as well as generalization to unseen examples (Ioffe and Szegedy 2015).

Depending on the number of outer, reducing, and inner layers our model has approximately $2.3 \cdot 10^5$ to $2.1 \cdot 10^6$ parameters. Dimension of the latent space however is solely regulated by the number of reducing layers N_{reduce} and amounts to $256 \cdot 4^{N_{reduce}}$. It ranges from a minimum of 256 (zero reducing layers) up to 262144 (five reducing layers). Notice that the Red Sea downsampled spatial dimensionality of input data is around 1855, so our architecture is employed in all regimes ranging from reducing to expanding spatial dimensionality in its latent space. The number of temperature anomaly datapoints available for training is daily data matrix size multiplied by the number of days and the average percentage of available data which equals around $1.4 \cdot 10^7$ numbers. The available data is one to two orders of magnitude larger than the number of model parameters, so we are confident our models do not overfit.

Input dimensionality. Using multi-day input for training the model to predict the day in the middle of the input block allows the model to utilize the rate of change in time and learn correlations in short time scales. We further find that providing masks as input in addition to anomaly data improves training. Additionally, positional encoding is concatenated to input data as two additional channels provided to the first convolutional layer (so $d_{in} = 2N_{days} + 2$). Positional encoding provides information about geographical latitude and longitude as horizontal and vertical linear sweep of real numbers between -1 and 1 .

For all our models we use positional encoding and provide $N_{days} = 3$ consecutive days at input, so the number of input channels at the first convolutional layer is $d_{in} = 8$ accounting for 3 data channels, 3 mask channels, and 2 positional encoding channels.

Loss function and norm Seeing as the marginal distribution of the provided real-world data is approximately Gaussian, it would be reasonable to use the L^2 norm as the optimization goal in (1) because it should minimize deviation of predictions with regard to actual values. Intriguingly, in our experiments we find almost no difference in the L^1 validation loss when L^1 cost function was used as opposed to the L^1 validation loss when the L^2 cost function was optimized. We conservatively decided to use the L^1 cost function to obtain possibly larger reconstruction errors but also capture a larger variance of extreme values.

Optimizer hyperparameters. Models are trained using the fast.ai library (Howard et al. 2018). For the optimizer we employ a synergistic approach provided by the Ranger algorithm (Wright et al. 2019). In order to stabilize the start of the training process, Ranger relies on the Rectified Adam (RAdam) optimizer (Liu et al. 2020) which in turn is a modified adaptive moment estimation optimizer (Kingma and Ba 2017) with a starting warmup period. Additionally, to stabilize the rest of the training, parameter lookahead avoids overshooting good local minima in parameter space (Zhang et al. 2019). Flat-cosine one-cycle policy for learning rate and weight decay ensures fast convergence to a broad optimum which allows the trained model to generalize well (Smith 2018).

The following RAdam hyperparameters in particular influence the length and generalizability of the trained model: maximum learning rate, weight decay factor, exponential decay rates of the first and second moments, number of epochs per training and training batch size. We fixed maximum learning rate to 0.003, the number of epochs to 50, and the exponential decay rates to $\beta = (0.95, 0.999)$. Additionally, we regard dropout percentage as an optimizer hyperparameter.

To suitably tune weight decay, batch size and dropout hyperparameters, a heuristic meta-optimization scheme was devised and successfully used to train our models. In order to avoid over- or under-fitting, each model is trained through several iterations of 50 epochs until we achieve a satisfactory ratio between validation and training losses between 1 and 1.05. We start the first iteration of model training with fixing dropout to 0, weight decay to 0.3 and batch size to 32. In each iteration, until we reach satisfactory validation and training loss ratio, we either decrease or increase regularization, depending on whether validation and training loss ratio is less than 1 or greater than 1.05. To decrease regularization we consider between decreasing dropout, decreasing weight decay or decreasing batch size. Notice that since we use batch normalization in each convolutional layer, slightly decreasing batch size from the initial value seems to actually decrease and not increase regularization as expected. To increase regularization we consider between increasing dropout or increasing weight decay. If we get the validation and training loss ratio in one iteration step less than 1, and in the next step greater than 1.05, or vice versa, we consider for the following iteration a weighted linear interpolation of dropout and weight decay hyperparameters from previous iterations. At the end of this process we select the model snapshot with the the lowest validation

loss evaluated, only over data in validation set that our model actually reconstructed, that is, we calculated the validation loss using the mask $m_{\text{orig}}^{(n)} - m'^{(n)}$ as a relevant metric for the quality of missing data reconstruction. We consider such a model to be well-trained.

Prediction ensembling. One of the most important aspects that we use in our method is independent training of an ensemble of models with different convolutional autoencoder hyperparameters. A number of predictions for missing temperature anomaly values are inferred from each of the well-trained models. Afterwards, all of those predictions are ensembled to calculate the empirical distribution of wanted temperature anomaly extremes.

4 Results and Discussion

For the solution of Data Challenge problem we ensemble predictions made by a set of 155 models with different combinations of convolutional autoencoder hyperparameters that satisfy $1 \leq N_{\text{outer}} + N_{\text{reduce}} + N_{\text{inner}} \leq 10$, with $N_{\text{outer}} \geq 1$, $0 \leq N_{\text{reduce}} \leq 5$ and $N_{\text{inner}} \geq 0$. Each model was trained independently using the described meta-optimization scheme to select optimizer hyperparameters that produce well-trained models. For the worst case model meta-optimization scheme converged to well-trained model in at most 13 iterations. On average it took 3.27 iterations of meta-optimization to reach a well-trained model, for a cumulative of 507 trained models. For only one out of 155 final models, the algorithm failed to achieved the targeted validation and training loss ratio which ended at only 1.09.

Measured on a quad-core computer system with Nvidia RTX 2070 8 GB RAM GPU, worst-case training time per model and per one iteration of meta-optimization scheme was around 1 hour and 20 minutes. The average training time was around 43 minutes. Cumulative training time for the full ensemble of 155 well-trained models was approximately 15 days.

For every of 155 trained models, 20 full historical predictions were inferred with a total of 3100 complete spatio-temporal reconstructions of Red Sea temperature anomalies. These were used in place of missing data to calculate the empirical distribution of temperature anomaly extremes over space and time at locations specified by the Data Challenge problem. Timed on the above equipment, this operation took about 20 minutes per model and finished in about 2 days for all 155 models.

In the end we calculated the $\overline{\text{twCRPS}}$ score to be $3.618 \cdot 10^{-4}$.

As a contrast, in our original second place solution to the Extreme Value Analysis 2019 Data Challenge we also used an ensemble of predictions, but it used only 8 models. These models were all trained and evaluated with similar convolutional autoencoder hyperparameters but on full-resolution data without resampling, using single-day input and no positional encoding. They were trained with the Adam optimizer (Kingma and Ba 2017) without hyperparameter tuning, and at that time we were using both L^1 and L^2 norms for model

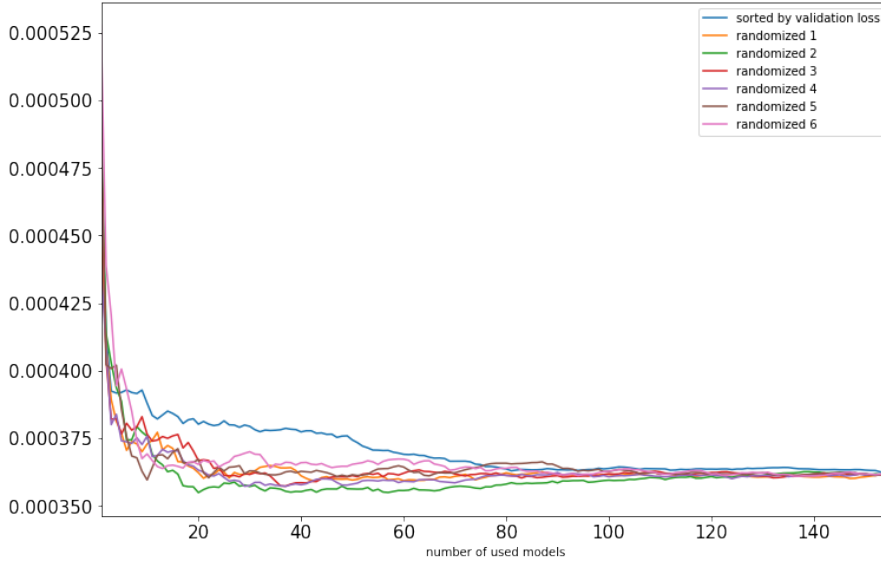


Fig. 2 Graph of the $\overline{\text{twCRPS}}$ score of a sub-ensemble prediction depending on the number of models used to form sub-ensemble. The models are either sorted ascending by validation loss evaluated at additionally damaged data or the order is randomized. The first M models are chosen for each sub-ensemble.

training. Then we reached the $\overline{\text{twCRPS}}$ score of $4.667 \cdot 10^{-4}$, so our current result is a significant improvement.

What happens if we try to take a smaller ensemble of predictions? The ensemble produced by 155 models takes quite a long time to train and evaluate. It is possible that a smaller ensemble could have comparable performance regarding the $\overline{\text{twCRPS}}$ score.

First let us consider only a trivial ensemble created by a single model. Let us take what we consider the best well-trained model out of all 155 models, ie. the model with lowest validation loss evaluated at additionally damaged data $m_{\text{orig}}^{(n)} - m'^{(n)}$. Let us sample from this model full 3100 data reconstructions, the same number of samples as the previously discussed large ensemble. We get the modest $\overline{\text{twCRPS}}$ score of $4.804 \cdot 10^{-4}$, which means that our large ensemble indeed helps improve the prediction quality over a single best-performing model. Notice that taking 3100 samples for a single model does not significantly improve the score when compared to only 20 samples ($4.802 \cdot 10^{-4}$).

Next, let us consider a family of ensembles, each ensemble a sub-ensemble consisting of the first M out of 155 well-trained models. For $M = 1$ we get the trivial ensemble already considered, and for $M = 155$ we get the full ensemble. For comparison, let us take a couple of randomized model orders and produce the same sub-ensembles, by taking only the first M out of 155 models, see Figure 2. Random picking the sub-ensemble wins over ordered picking, but we

still have to put quite a large number of models into our ensemble to get close to the twCRPS score achieved using all of 155 models.

The meta-optimization scheme which tunes optimizer hyperparameters clearly helps with the quality of prediction. To illustrate this we took 155 models trained for 50 epochs once, using fixed optimizer hyperparameters without any additional tuning. Many of these models were over- or under-trained. We calculated the twCRPS score to be $3.970 \cdot 10^{-4}$, meaning that proper hyperparameter selection and well-trained models improve the score by about 10%.

Training a large ensemble of models is prohibitively expensive regarding computation time and resources. Therefore it is difficult to investigate the impact of each decision in selecting individual model hyperparameters. It is far from clear which hyperparameters (number of layers, kernel size, number of channels, number of days at input...) had the greatest impact on the improvement of our prediction. A detailed ablation study with a full-blown set of models unfortunately may well require months or years to train and evaluate using our currently available hardware.

Figure 2 indicates that a randomly chosen ensemble of only about 25 out of 155 current models could prove sufficient for an ablation study. We have indeed made first attempts in that direction by selecting 5 different models as templates and varying $d_{ch} \in \{64, 128, 256\}$, $N_{days} \in \{1, 3, 11\}$ as well as whether positional encoding is used. This resulted in 90 well-trained models partitioned in 18 different ensembles. Despite each ensemble containing only 5 different models, there are preliminary indications that positional encoding is very helpful and that a large block of $N_{days} = 11$ at the input performs better than $N_{days} \in \{1, 3\}$.

The presented technique relies on a suitable choice of masks that describe additional damage. In domains where such data loss is easily generated, such as tabular data or low-dimensional time series, our technique could prove to be useful. For image-like datasets found in medicine, geology, climatology, etc., an extensive study is needed to assess the influence of added damage and the distribution of imputed noise on the quality of recovered data.

We also note there are other viable model architectures that ought to be explored. For instance, in this work we use the simplest convolutional layers for our autoencoder. Instead, better generalization might be obtained using ResNet (He et al. 2015) or UNet architectures which use skip connections as high-resolution pathways between distant layers (Ronneberger et al. 2015). In particular, U-Net places skip connections between corresponding encoder and decoder layers to preserve fine detail. Even though it is originally used for medical image segmentation or classification, U-Net might prove to be a good fit for regression problems such as ours as it is eg. used to model MisGAN’s generators (Li et al. 2019). Going further, in our dataset possibly the largest source of untapped information lie in long-term temporal correlations which we currently underutilize. A more extensive study of time-domain information is needed. Here, image latent space could be used as input to dedicated recurrent neural networks or even novel attention-based models currently explored by the natural language processing community Vaswani et al. (2017).

5 Concluding remarks

In this work we present a solution to the Extreme Value Analysis 2019 Data Challenge. A technique is described to recover missing data by training an ensemble of models on additional data damage we introduce ourselves. Sampling from autoencoder-like approximations of observed data distributions provides a feasible way to analyze complex dynamics of geophysical phenomena. The described approach seems amenable to be applied in other areas of basic and applied research with rare and extreme events.

Acknowledgements We thank Ivan Balog for enlightening discussions.

Conflict of interest

The authors declare that they have no conflict of interest.

References

- Asadi R, Regan A (2019) A convolution recurrent autoencoder for spatio-temporal missing data imputation. URL <http://arxiv.org/abs/1904.12413v1>; <http://arxiv.org/pdf/1904.12413v1>, 1904.12413v1
- Behnke S (2003) Hierarchical Neural Networks for Image Interpretation, Lecture Notes in Computer Science, vol 2766. Springer
- Cao W, Wang D, Li J, Zhou H, Li L, Li Y (2018) Brits: Bidirectional recurrent imputation for time series. Advances in Neural Information Processing Systems 31 pp 6775–6785, URL <http://papers.nips.cc/paper/7911-brits-bidirectional-recurrent-imputation-for-time-series>
- Che Z, Purushotham S, Cho K, Sontag D, Liu Y (2018) Recurrent neural networks for multivariate time series with missing values. Scientific Reports 8(1):6085–, DOI 10.1038/s41598-018-24271-9
- Goodfellow I, Bengio Y, Courville A (2016) Deep Learning. Adaptive computation and machine learning, MIT Press, URL <http://www.deeplearningbook.org>
- Goodfellow IJ, Pouget-Abadie J, Mirza M, Xu B, Warde-Farley D, Ozair S, Courville A, Bengio Y (2014) Generative adversarial networks. URL <http://arxiv.org/abs/1406.2661>, cite arxiv:1406.2661
- He K, Zhang X, Ren S, Sun J (2015) Deep residual learning for image recognition. URL <http://arxiv.org/abs/1512.03385>, cite arxiv:1512.03385Comment: Tech report
- Howard J, et al. (2018) fastai. <https://github.com/fastai/fastai>
- Huser R (2020) Editorial: Eva 2019 data competition on spatio-temporal prediction of red sea surface temperature extremes. Extremes DOI 10.1007/s10687-019-00369-9, URL <https://doi.org/10.1007/s10687-019-00369-9>

- Ioffe S, Szegedy C (2015) Batch normalization: Accelerating deep network training by reducing internal covariate shift. URL <http://arxiv.org/abs/1502.03167>, cite arxiv:1502.03167
- Kingma DP, Ba J (2017) Adam: A method for stochastic optimization. URL <http://arxiv.org/abs/1412.6980v9>; <http://arxiv.org/pdf/1412.6980v9>, 1412.6980v9
- Klambauer G, Unterthiner T, Mayr A, Hochreiter S (2017) Self-normalizing neural networks. In: Advances in neural information processing systems, pp 971–980
- Kramer M (1991) Nonlinear principal component analysis using autoassociative neural networks. *AICHE Journal* 37:233–243
- Krizhevsky A, Sutskever I, Hinton GE (2012) Imagenet classification with deep convolutional neural networks. *Advances in Neural Information Processing Systems* 25:1106–1114, URL <https://papers.nips.cc/paper/4824-imagenet-classification-with-deep-convolutional-neural-networks.pdf>
- Le T, Nguyen TD, Phung D (2017) Kgan: How to break the minimax game in gan. arXiv preprint arXiv:171101744
- Lee JW, Park SC (2015) Artificial neural network-based data recovery system for the time series of tide stations. *Journal of Coastal Research* 32(1):213–224, DOI 10.2112/JCOASTRES-D-14-00233.1, URL <https://doi.org/10.2112/JCOASTRES-D-14-00233.1>, https://meridian.allenpress.com/jcr/article-pdf/32/1/213/1648085/jcoastres-d-14-00233_1.pdf
- Li SC, Jiang B, Marlin BM (2019) Misgan: Learning from incomplete data with generative adversarial networks. CoRR abs/1902.09599, URL <http://arxiv.org/abs/1902.09599>, 1902.09599
- Liu L, Jiang H, He P, Chen W, Liu X, Gao J, Han J (2020) On the variance of the adaptive learning rate and beyond. URL <http://arxiv.org/abs/1908.03265v3>; <http://arxiv.org/pdf/1908.03265v3>, 1908.03265v3
- Nitish S, Hinton G, Krizhevsky A, Sutskever I, Salakhutdinov R (2014) Dropout: A simple way to prevent neural networks from overfitting. *Journal of Machine Learning Research* 15(56):1929–1958, URL <http://jmlr.org/papers/v15/srivastava14a.html>
- Paszke A, Gross S, Massa F, Lerer A, Bradbury J, Chanan G, Killeen T, Lin Z, Gimelshein N, Antiga L, Desmaison A, Köpf A, Yang E, DeVito Z, Raison M, Tejani A, Chilamkurthy S, Steiner B, Fang L, Bai J, Chintala S (2019) Pytorch: An imperative style, high-performance deep learning library. In: Wallach HM, Larochelle H, Beygelzimer A, d’Alché-Buc F, Fox EB, Garnett R (eds) *Advances in Neural Information Processing Systems 32: Annual Conference on Neural Information Processing Systems 2019, NeurIPS 2019, 8-14 December 2019, Vancouver, BC, Canada*, pp 8024–8035, URL <http://papers.nips.cc/paper/9015-pytorch-an-imperative-style-high-performance-deep-learning-library>
- Ronneberger O, Fischer P, Brox T (2015) U-net: Convolutional networks for biomedical image segmentation. In: Navab N, Hornegger J, Wells WM,

- Frangi AF (eds) Medical Image Computing and Computer-Assisted Intervention – MICCAI 2015, Springer International Publishing, Cham, pp 234–241, DOI 10.1007/978-3-319-24574-4_28
- Rossiev A, Makarenko N, Kuandykov Y, Dergachev V (2002) Recovering data gaps through neural network methods. *International Journal of Geomagnetism and Aeronomy* 3:191–197
- Schlemper J, Caballero J, Hajnal JV, Price A, Rueckert D (2017) A deep cascade of convolutional neural networks for mr image reconstruction. URL <http://arxiv.org/abs/1703.00555v1>; <http://arxiv.org/pdf/1703.00555v1>, 1703.00555v1
- Smith LN (2018) A disciplined approach to neural network hyper-parameters: Part 1 - learning rate, batch size, momentum, and weight decay. CoRR abs/1803.09820, URL <http://arxiv.org/abs/1803.09820>, 1803.09820
- Vaswani A, Shazeer N, Parmar N, Uszkoreit J, Jones L, Gomez AN, Kaiser Ł, Polosukhin I (2017) Attention is all you need. In: Guyon I, Luxburg UV, Bengio S, Wallach H, Fergus R, Vishwanathan S, Garnett R (eds) *Advances in Neural Information Processing Systems* 30, Curran Associates, Inc., pp 5998–6008, URL <https://papers.nips.cc/paper/7181-attention-is-all-you-need>
- Wei X, Gong B, Liu Z, Lu W, Wang L (2018) Improving the improved training of wasserstein gans: A consistency term and its dual effect. URL <http://arxiv.org/abs/1803.01541v1>; <http://arxiv.org/pdf/1803.01541v1>, 1803.01541v1
- Wright L, et al. (2019) Ranger. <https://github.com/lessw2020/Ranger-Deep-Learning-Optimizer>
- Zhang MR, Lucas J, Hinton G, Ba J (2019) Lookahead optimizer: k steps forward, 1 step back. URL <http://arxiv.org/abs/1907.08610v2>; <http://arxiv.org/pdf/1907.08610v2>, 1907.08610v2
- Zhang W (1988) Shift-invariant pattern recognition neural network and its optical architecture. In: *Proceedings of Annual Conference of the Japan Society of Applied Physics*